CARRIER DENSITY AND TRANSPORT GOVERNED OPTICAL NONLINEARITIES IN BULK SEMICONDUCTORS[1]

M. SUDZIUS, K. JARASIUNAS

Institute of Materials Science and Applied Research, Vilnius University
(Sauletekio Ave., 9, Bld. 3, LT-10222 Vilnius, Lithuania; e-mail: markas.sudzius@ff.vu.lt)

UDC 621.315.592

Development of four-wave mixing techniques on free carrier and photorefractive transient gratings in bulk semiconductor materials is given. Experimental studies together with numerical modeling allowed us to demonstrate a feasibility of the nanosecond and picosecond dynamic grating techniques for the control over semiconductor wafer quality, to investigate the room-temperature photoquenching of EL2 defects in GaAs, as well as to reveal conditions for the very effective feedback effect of a space-charge field on the carrier transport in variously doped GaAs, CdTe, and ZnTe crystals.

Introduction

Recent studies of light interaction with matter furthered the deeper understanding in optical nonlinearities and developed methods of nonlinear spectroscopy as well as engineering applications [1]. Nonlinear optical techniques, based on a strong correlation between electrical and optical processes, opened a possibility to analyze electrical processes in nondestructive "all-optical" way and to develop relevant measurement techniques for the studies of the nonequilibrium carrier dynamics. Due to the role of deep centers in compensation mechanisms of semiinsulating semiconductors, the optical studies of deep centers became of crucial importance [2–4]. In particular, the light-induced dynamic grating technique [5–7] has been demonstrated as a simple but powerful technique for the control over photoelectrical processes and transport in bulk crystals and at the surface. Recent studies however raised new questions, such as a search of semiconductors for a metastable operation at room temperature [8], investigation of the metastable grating dynamics [9], role of compensation ratio in this effect [10], etc. On the other hand, an important question is the compensation mechanisms of semiconductors by which an undoped material becomes semiinsulating [11]. All these questions, in turn, require a deeper understanding in the nonlinear excitation-dependent deep-trap-assisted generation and recombination of carriers, as well as in their transport.

The present paper focuses on the application of four-wave mixing (FWM) for the studies of carrier generation, transport, and recombination, as well as defect characterization via light diffraction in bulk GaAs:EL2 and variously doped CdTe:V and ZnTe crystals. A short review of most recent FWM results on layered structures and novel devices for a nondestructive control over semiconductors is given.

1. Dynamic Gratings: Basic Principles and Advantages

Light diffraction by light-induced dynamic gratings has been an object of intensive studies a decade ago (see review papers [5, 6, 12]). A particular advantage of this technique is its capability to monitor the carrier generation, transport, and recombination, as it bridges the photoelectrical properties of semiconductors with related optical nonlinearities which are monitored by means of time-resolved dynamic holography. The latter approach — excitation of a crystal with light interference pattern — has a number of advantages against the other "excite-probe" techniques. First of all, the light diffraction creates new beams in a dark field, thus increasing the signal-to-noise ratio. Next, the intensity of diffracted beams nonlinearly reflects the modulation amplitude of the refractive index. In addition, a spatial modulation of the carrier density allows a simple monitoring of diffusion processes along the grating vector by varying the grating period, and, thus, enables the separation of diffusion from recombination. Finally, a variation of the excitation wavelength leads to various thicknesses of the photoexcited region. The spatial in-depth resolution is defined by thickness of a bulk crystal, if it is excited by a quantum with energy $h\nu < E_g$, and may reach a submicron thickness at strong light absorption ($h\nu > E_g$). In-plane resolution is limited by

[1] This article is dedicated to Professor Marat Soskin on the occasion of his 75th birthday.

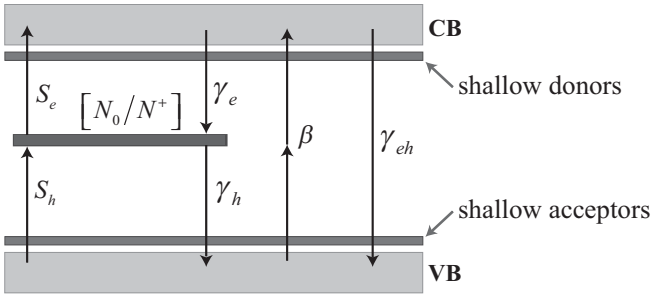

Fig. 1. Schematic energy-level diagram showing the processes of photoionization of a deep trap (S_e, S_h), two-photon absorption (β) as well as free carrier linear (γ_e, γ_h) and bimolecular (γ_{eh}) recombination

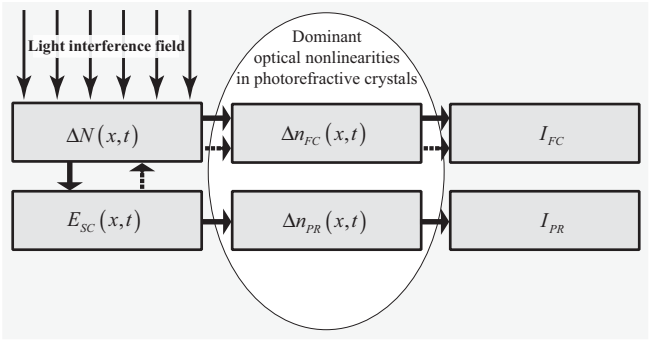

Fig. 2. Mechanisms of refractive index modulation in photorefractive crystals and the feedback effect of the space-charge field on free carrier transport

the number of grating lines in the excited spot and varies from 50 μm to 1 mm.

From the point of view of materials research, the most important part of this technique is the set of material equations, which joins quantitatively the generation, recombination, and transport processes with the measured light diffraction characteristics, i.e. the grating kinetics at various periods and excitation intensities, dependence of diffraction efficiency on excitation intensity [13]. In many cases, the simple one-level model is capable to explain many effects which might occur in photorefractive crystals. Energy diagram of the model is sketched in Fig. 1. The processes shown can be described by a system of material equations [14–16]: the continuity and current density equations for electrons (n) and holes (p), the rate equation for the ionized trap density (N^+), and the Poisson equation for the space-charge (SC) field $E_{\rm SC}$:

$$\frac{\partial n}{\partial t} = \frac{S_{\rm e} I N_0}{h\nu} + \frac{\beta I^2}{2h\nu} + \frac{1}{e}\frac{\partial j_{\rm e}}{\partial x} - \gamma_{\rm e} n N^+ - \gamma_{\rm eh} n p\,, \quad (1)$$

$$\frac{\partial p}{\partial t} = \frac{S_{\rm h} I N^+}{h\nu} + \frac{\beta I^2}{2h\nu} - \frac{1}{e}\frac{\partial j_{\rm h}}{\partial x} - \gamma_{\rm h} p N_0 - \gamma_{\rm eh} n p\,, \quad (2)$$

$$\frac{\partial N^+}{\partial t} = \frac{S_{\rm e} I N_0}{h\nu} - \frac{S_{\rm h} I N^+}{h\nu} - \gamma_{\rm e} n N^+ + \gamma_{\rm h} p N_0\,, \quad (3)$$

$$j_{\rm e} = e n \mu_{\rm e} E_{\rm SC} + \mu_{\rm e} k_{\rm B} T \frac{\partial n}{\partial x}, \quad (4)$$

$$j_{\rm h} = e p \mu_{\rm h} E_{\rm SC} - \mu_{\rm h} k_{\rm B} T \frac{\partial p}{\partial x}, \quad (5)$$

$$\frac{\partial E_{\rm SC}}{\partial x} = \frac{-e}{\varepsilon_0 \varepsilon_{\rm r}} \left(n + N_{\rm A} - p - N^+\right). \quad (6)$$

Here, the excitation term I has the spatial periodicity of Λ and corresponds to the light interference field of two laser pulses with a Gaussian temporal shape $f(t)$:

$$I(x,t) = I_0 f(t) \left[1 + m\cos\left(K_g x\right)\right] \quad (7)$$

with I_0 as a photon flux, m as a modulation depth of the fringes, and $K_g = 2\pi/\Lambda$ as a grating vector.

It goes without saying that the *a priori* knowledge of the dominant refractive index modulation mechanism under the conditions of experiment is of the utmost importance. Fig. 2 shows dominant mechanisms of refractive index modulation in photorefractive crystals. As a rule, in the spectral region below the bandgap, the free carrier nonlinearity is dominant with refractive index modulation $\Delta n_{\rm FC}$ prevailing over free carrier absorption $\Delta k_{\rm FC} = \Delta\alpha_{\rm FC}\lambda/4\pi < \Delta n_{\rm FC}$. However, the recharge of deep traps in photorefractive crystals and the subsequent absorption index spatial modulation should be also considered. The refractive index modulation by free carriers $\Delta n_{\rm FC} = n_{eh}\Delta N_{e,h}$ is given by the well-known Drude—Lorentz model with the refractive index modulation coefficient by one electron-hole pair n_{eh} [5, 6]:

$$\Delta n_{\rm FC} \approx -\frac{e^2}{2n_0\varepsilon_0 m_0 \omega^2}\left(\frac{\Delta n}{m_e^*} + \frac{\Delta p}{m_h^*}\right). \quad (8)$$

It is seen that electrons dominate in the refractive index modulation, even at the bipolar carrier generation, because $m_e^* < m_h^*$.

The space-charge field $E_{\rm SC}$ gives rise to an index grating of different origin through the linear electro-optic effect (Pockels effect) [13]. When $\mathbf{E}_{\rm SC}$ is oriented along a $\langle 100\rangle$ axis of the crystal, the change in the refractive index is given by

$$\Delta n_{\rm PR} = -\frac{1}{2} n_0^3 r_{41} E_{\rm SC}\,, \quad (9)$$

where r_{41} is the electro-optic coefficient.

The value of refractive index modulation n_{eh} varies in the range of $(4 \div 7) \times 10^{-21}\,{\rm cm}^3$ (for CdTe, GaAs,

GaN) at a wavelength of 1.06 μm of the probe beam. This coefficient together with the thickness of the excited region d determines the sensitivity of the technique, i.e. the minimum value of product Δnd, which can be detected in diffraction. Usually, the signal-to-noise ratio of ≈ 1 is reached at the diffraction efficiency $\eta \cong 10^{-5}$, which corresponds to $\Delta nd \geq 1 \times 10^{-3}$ μm, and this limit corresponds to the lowest carrier density of 10^{15} cm^{-3} in a few mm thick bulk crystals which can be assessed by the FWM technique.

2. Instrumentation and Configurations of FWM

Fig. 3 shows a configuration of the optical scheme and instrumentation, used for the recording and probing of free carrier (FC) and photorefractive (PR) gratings in bulk crystals. The scheme presents a common configuration of degenerate four-wave mixing (DFWM), involving a combination of four waves whose wavelengths are equal: the forward s-polarized waves record a grating in the bulk and the backward delayed probe wave monitors the grating decay. Contribution of photorefractive and free carrier gratings can be separated by choosing the s- or p-polarization state of the probe beam, respectively [17,18]. The diffracted wave counterpropagates to one of the recording beams at the Bragg-matched angle and is extracted by a Glan prism. The scheme allows the extraction of all the diffracted beam intensity which may reach 100 % of the probe beam for light diffraction by a thick grating.

The DFWM is used to study cases of weak interaction in bulk crystals, such as the deep impurity-related carrier generation in semiinsulating materials or two-photon interband transitions. In turn, a non-degenerate four-wave mixing is often used as a powerful technique to investigate optical and electrical properties of semiconductors at the surface [19]. The beams at wavelengths above E_g are used to record the free carrier grating, while the probe beam wavelength is in the transparency region of a crystal. The carriers are created optically at the very surface with the excitation depth d_{eff} being close to the inverse absorption coefficient of recording beams. Further bipolar diffusion of carriers to the sample depth can significantly expand the excited area into the bulk of crystals. A delayed probe beam monitors the electron-hole density as a function of time via the time-varying diffraction efficiency of the grating. In case of the surface excitation, the regime of a thin grating takes place and the direction of the probe is not constrained any more by the Bragg-matching condition

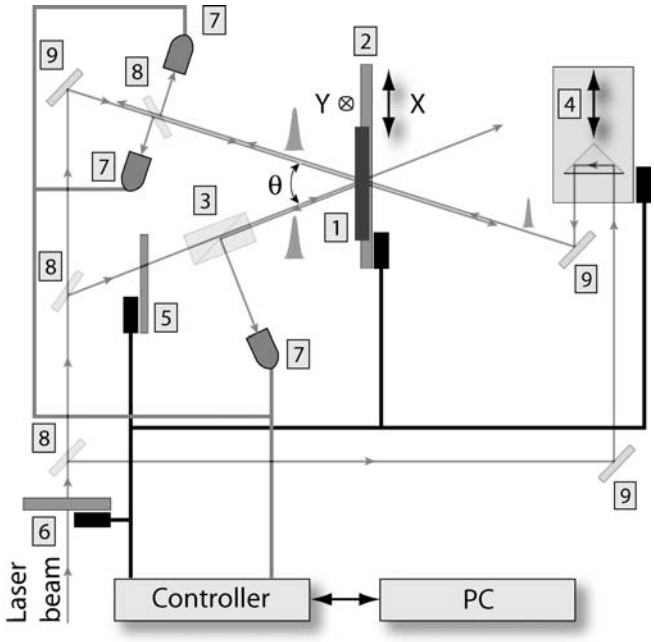

Fig. 3. Scheme of a four-wave mixing setup. The elements shown are: *1* — Sample, *2* — Translation stages, *3* — Glan prism, *4* — Delay line of the probe beam, *5* — Shutter, *6* — Attenuator, *7* — Detectors, *8* — Beam splitters, *9* — Dielectric mirrors

(the factor $Q = 2\pi\lambda d/\left(n\Lambda^2\right) \leq 1$) [6]. Therefore, the diffracted beams can be observed in the dark field of diffraction. This configuration has been applied initially to determine the surface recombination velocities in GaAs and InP crystals [19].

The diffraction efficiency of either grating can be described as $\eta \approx \left(\pi\Delta nd/\lambda\right)^2$, where Δn stands for refractive index modulation. The decay time of the grating efficiency $\eta\left(t\right) \propto \exp\left(-2t/\tau_G\right)$ corresponds to time interval $\Delta t = \tau_G$, in which the η value decreases by e^2 times, while the carrier modulation decreases by e times in this time interval. A plot in the form $1/\tau_G = f\left(\left(2\pi/\Lambda\right)^2\right)$ allows the separation of diffusion processes from the carrier recombination, as the inverse of $\tau_G\left(t\right)$ is the sum of two decay processes of spatial carrier modulation:

$$1/\tau_G = 1/\tau_R + 1/\tau_D \tag{10}$$

where τ_R is the recombination time and $\tau_D = \Lambda^2/\left(4\pi^2 D\right)$ is the diffusion time of the grating erasure. The slope of the plot provides D value, while the intersection with the ordinate axis — the $1/\tau_R$ value.

In our experiments, we used a nanosecond Q-switched or picosecond mode-locked Nd:YAG laser to

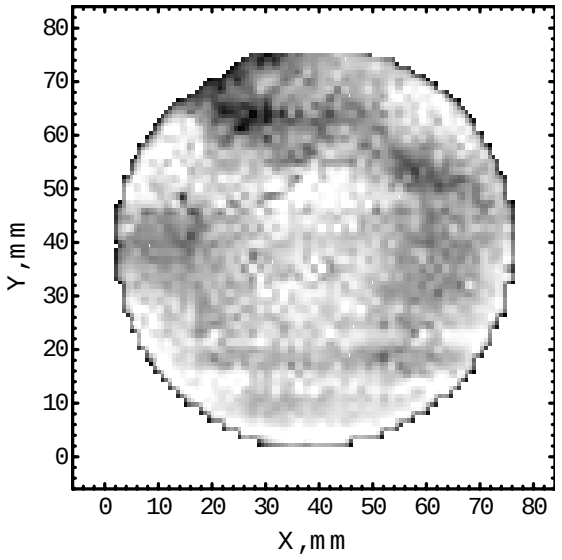

Fig. 4. Map of FC diffracted signal in GaAs:EL2 wafer at $\lambda = 1064\,\text{nm}$ wavelength: dark areas correspond to lower density of defects

record and probe the gratings. The picosecond laser (model PL-2143, Expla Co.) also emits the second (532 nm) and third (355 nm) harmonics. A parametric generator PG-401 (Expla Co.), emitting in the spectral range from 420 to 2000 nm, was used to record gratings in bulk ZnTe crystals, and the grating decay was monitored by the delayed beam of a PL-2143 laser at 1064 nm. The intensities of recording I_0, probing I_p, transmitted probe I_{pT}, and diffracted I_1 beams are controlled by Si photodiodes, and the data acquisition system measures the instantaneous diffraction efficiency of the grating $\eta(t) = (I_1 - I_s)/I_{pT}$ (extracting the scattered background signal I_s from the diffracted beam) and transmission of the sample $T(t) = I_{pT}/I_p$.

3. Bulk Semiconductors: Modeling and Experimental Studies

3.1. Spatial Distribution of EL2 in GaAs Wafers

Optical and electrical properties of undoped semiinsulating GaAs crystals grown by the liquid encapsulated Czochralski or Bridgman technique are determined by intrinsic EL2 donors located at 0.75 eV below the bottom of the conduction band [4]. Typical concentration of EL2 defects is $N_T \approx (1 \div 2) \cdot 10^{16}\,\text{cm}^{-3}$ [11]. The semiinsulating character of such a crystal is due to the compensation of residual shallow acceptors by EL2 donors, where the Fermi level is pinned. Thus, EL2 are both in neutral $EL2^0$ and ionized $EL2^+$ states [10,20].

In semiinsulating GaAs crystals, the presence of EL2 is detected by the optical absorption at 1.06 μm which can be enhanced by nonlinear technique. Since, at this wavelength, the optical cross-section for transitions from the valence band to ionized EL2 is much smaller than that for the transitions from neutral EL2 to the conduction band [21], one can attribute the absorption at 1.06 μm to neutral EL2 centers. In that view, the FC nonlinearity should be very sensitive to the crystal compensation ratio by EL2 defects R which is usually defined as the ratio between the acceptor concentration N_A and the total density of EL2 defects N_T. On the other hand, it is well known that there is a strong correlation between EL2 and the dislocation distribution [11, 22, 23] in GaAs due to impurity atmosphere associated with dislocations. This correlation has been proven by comparison of nondestructive measurements with the EPD distribution revealed by KOH-etching [23, 24]. Thus, a monitoring of the dislocation density across a GaAs wafer via the EL2 atmosphere around dislocations is possible by nonlinear optical techniques [25, 26].

Studies of the uniformity of GaAs wafers and the distribution of carrier lifetime across the substrate have been performed and revealed a W-like spatial distribution of light diffraction efficiency and carrier lifetime [22, 23, 25, 26]. As an example, Fig. 4 shows the spatial distribution of FC diffracted signals which corresponds to the EL2 distribution in semiinsulating GaAs [26]. The measurement was performed in a 3-inch diameter, undoped GaAs crystal grown by the liquid-encapsulated Czochralski technique. A grating with 18 μm spacing was recorded and probed simultaneously by 12-ns laser pulses. The sample was moved in the X-Y plane with 1 mm step in both directions thus allowing us to record the maps of transmitted or diffracted signals.

Much broader range of effects can be explored in time-resolved measurements of a picosecond FC grating decay by simply varying the grating period or a delay of the probe beam. In Fig. 5, we show the recombination-governed and transport-governed decay of FC gratings in some characteristic areas of a SI GaAs wafer: at the center and at the edge, where the dislocation density is the highest, and at the half-radius of a wafer, where the defect density is the lowest [27]. A regime of the recombination-governed decay can be realized for large grating periods. In this case, the dynamics of diffraction efficiency yields the carrier lifetime which is shorter in

the areas of higher sample transmittivity, i.e. where the density of $EL2^+$ states N^+ is higher [28]. On the other hand, the transport-governed FC grating decay can be achieved if small grating periods are used. In this case, the dynamics of transient grating reveals a substantial role of the light-created space-charge field on the diffusive carrier transport [23]: the higher the EL2 density in its neutral state N^0, the larger is the SC field which compensates the diffusive decay of the grating by electron drift in the field established between the ionized EL2 states and electrons. At even higher excitations, a Dember field between mobile carriers obscures the role of deep defects.

3.2. Optical Nonlinearities at Transient Quenching of EL2 Defect

Among the other properties of deep EL2 donor in semiinsulating GaAs crystals, the optical quenching of this defect has deserved attention as a novel way to realize the low-temperature photorefractive effect and enhance an internal space charge field [9, 29]. The latter effect is associated with the transfer of a defect from its neutral state to a metastable configuration EL2* under spatially nonuniform optical illumination, thus causing a local decompensation of shallow acceptors and p-type conductivity in illuminated areas. A spatial variation of the crystal conductivity leads to the Fermi level modulation and a corresponding enhancement of the internal SC field, seen in more efficient light diffraction [29, 30] or two-wave mixing [10] under steady-state conditions. The nature of the created SC field is different from that in the ordinary PR effect in semiinsulating GaAs, because light modifies not only the charge state of the EL2 defect, but also its concentration. Therefore, this effect is equivalent to the modulation doping by light and has both fundamental and applied interest.

Recently, we have investigated the carrier generation and transport under photoexcitation of a deep EL2 donor by nanosecond duration laser pulses, when photocarriers arise mainly from the photoionization of the deep donor [31]. The modeling of the EL2 density in its various states (neutral, ionized, and metastable), analysis of the spatial profiles of photogenerated carriers and the space charge field allowed us to determine conditions for the transient quenching of EL2 at 300 K and to reveal its influence on coexisting optical nonlinearities. We found a signature of EL2 photoquenching in the saturation of the diffraction

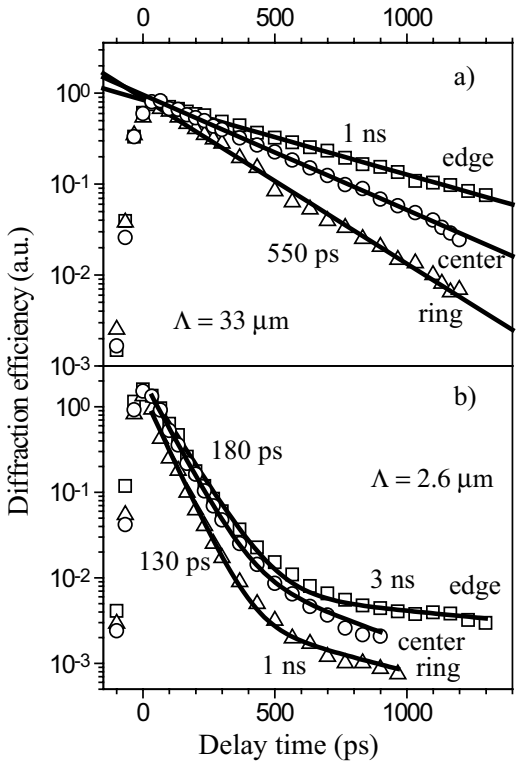

Fig. 5. Recombination-governed a and transport-governed b decay of the free carrier grating diffraction efficiency in some characteristic areas of a semiinsulating GaAs wafer

efficiency and the depletion of absorption at excitation energies below two-photon absorption. Comparison of the performed numerical analysis and DFWM experiments at 10-ns pulse excitation allowed us to verify the contribution of EL2 transient quenching to the free carrier nonlinearity.

In Fig. 6, we present the exposure characteristics of the light diffraction efficiency measured in an LEC-grown GaAs crystal. A power law dependence of diffraction efficiency as a function of excitation, $\eta \sim I_0^{\gamma}$, is typical with a slope $\gamma = \Delta \log(\eta)/\Delta \log(I_0)$. For free carrier gratings, the slope varies from $\gamma = 2$ for linear carrier generation [5] to $\gamma = 4$ for two-photon carrier generation [32]. In our case, the slope in the low excitation region equals to $\gamma = 1.6$, which points to the linear carrier generation from/via EL2 traps and a slight depletion of the trap density with excitation. The further essential saturation of diffraction efficiency with magnitude of $\gamma = 0.4$ is due to the very efficient depletion of deep traps because of the transfer of a considerable part of $EL2^0$ to the metastable state. A decrease of the absorption coefficient with intensity was also confirmed by the measured dependence of

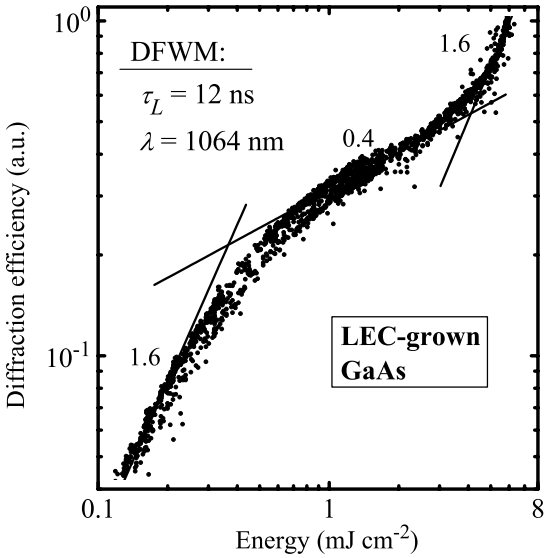

Fig. 6. Exposure characteristics of diffraction efficiency in an LEC-grown GaAs sample. The numbers mark the characteristic slopes of exposure characteristics for the certain energy interval

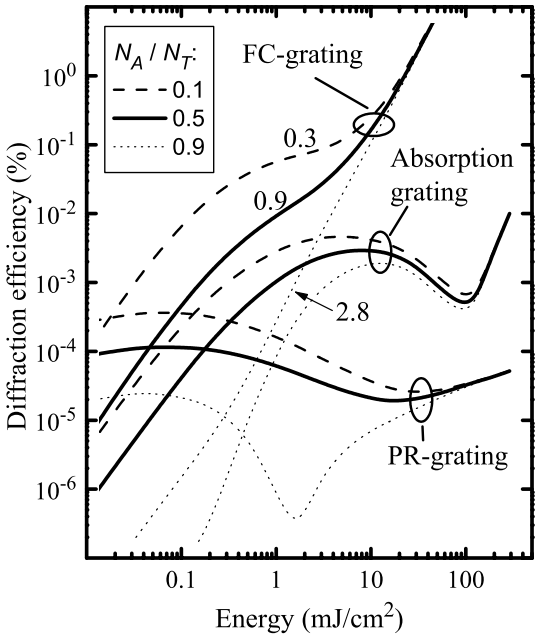

Fig. 7. Calculated exposure characteristics of the diffraction efficiency on FC, PR, and absorption gratings shown for three different compensation ratios by EL2 defects. Numbers indicate the EC extreme slope coefficients

transmittance as a function of excitation and pointed out to a decreased carrier generation rate in grating peaks. The further increase of the slope at an excitation energy above 5 mJcm^{-2} is probably related to the contribution of the other processes of carrier generation, as two-step transitions via a deep trap, the two-photon absorption or light-assisted recovery of a metastable state [33], which may provide neutral EL2 for the carrier generation.

The observed features of exposure characteristics are in good agreement with the results of numerical calculations. We have calculated the diffraction efficiencies of free carrier, photorefractive, and absorptive gratings for GaAs:EL2 bulk material of 1 mm thickness as a function of the excitation energy for 0.1, 0.5, and 0.9 crystal compensation ratios R by EL2 defects using the system of equations (1)—(6) complemented by the rate equation for the metastable EL2* state [31]

$$\frac{\partial N^*}{\partial t} = S_n^* I(N_0 - N^*) - (r + S_r^* I)N^*, \qquad (11)$$

where S_n^* is the optical metastable state generation cross section (EL2 $\rightarrow$ EL2* process) and S_r^* is the optical regeneration cross section (EL2 $\rightarrow$ EL2* process), whereas thermal recovery of the metastable state EL2* to the ground state is characterized by the thermal recovery rate r.

The calculated EC characteristics are shown in Fig. 7. The exposure characteristic of a free carrier grating show the tendency of saturation for $R = 0.1$ and $R = 0.5$ within the 0.5—5 mJcm^{-2} energy range and are enhanced for $R = 0.9$. The analysis of the spatial profiles of charges clearly indicated that the photoquenching of EL2 and a change of its charge state are responsible mechanisms for such a behaviour of FC diffraction efficiency. Therefore, the values of extreme slopes are very sensitive to the dark state compensation of the crystal as well as to the metastable transfer of EL2 defects [31].

The exposure characteristic of diffraction efficiency on a PR grating also carries information about the compensation level of the crystal. The origin of a SC field at low excitation is defined by dominant free carriers: if $R < S_n/(S_n + S_p)$, the electron generation dominates over the holes causing build-up of the SC field E_{SC1} between EL2$^+$ and mobile electrons [14, 26]; in opposite case, the SC field E_{SC2} is formed between the recharged EL2 and mobile holes and has opposite sign with respect to the E_{SC1} [31]. In addition, the field component E_D between mobile electrons and holes (Dember field) develops with excitation energy and has

spatial profile similar to that of E_{SC1}. In case of $R = 0.9$, the competition of E_{SC2} and E_D is clearly expressed as a dip in the diffraction efficiency on a PR grating. The dip is not observed for $R = 0.1$ and $R = 0.5$ EC curves since E_{SC1} and E_D are superimposed constructively.

The experimentally observed saturation of FC diffraction efficiency in GaAs crystals has suggested that the optically induced transfer of the EL2 to its metastable state is very efficient at 300 K and excitation above $1\,\mathrm{mJcm^{-2}}$. At $1.06\,\mu$m wavelength, $S_n^* = 1 \cdot 10^{-17}\,\mathrm{cm^2}$ is by two orders of magnitude larger than $S_r^* = 1 \cdot 10^{-19}\,\mathrm{cm^2}$ [10], which ensures the accumulation of the N^* density during excitation. The further dynamics of the N^* density is solely defined by thermal recovery of the EL2* population and is characterized by the thermal recovery rate r. For 80–140 K temperature interval, r is given by [34]

$$r = r_0 \exp\left(-\frac{E_r}{k_B T}\right), \qquad (12)$$

where r_0 is the vibrational-attempt-frequency and $E_r = 0.34\,\mathrm{eV}$ is the thermal activation energy of the recovery process. Reported values of r_0 differ from author to author and range from 8.6×10^{11} [35] to $1.6 \times 10^{12}\,\mathrm{s^{-1}}$ [36].

We have extended our studies of EL2 metastable transfer along with its recovery to the ground state at room temperature using time-resolved four-wave mixing [37]. Fig. 8 shows the experimentally measured diffraction efficiency vs. probe delay time as well as the calculated kinetics for different thermal recovery rates r. The energy of recording beams was $2\,\mathrm{mJcm^{-2}}$. The dashed line represents the case with no metastable transfer included. The scales of numerical and experimental results were equalized by applying a constant multiplier.

The two-exponential decay of the experimental curve is clearly seen: the fast initial part with ~ 9 ns decay time, which corresponds to bipolar diffusion of free carriers for 24 μm grating spacing is followed by the slow one with the decay time longer than 100 ns.

It was shown numerically that the space charge field cannot contribute to a slower grating decay at longer delay times as, under given experimental conditions, it decays also with bipolar diffusion time [37]. Therefore, the long living component is related to the recovery of a spatially photoquenched EL2 from the metastable to the ground state, which leads to the absorption index modulation and light diffraction on the amplitude grating. The best agreement between experimental and theoretical data is achieved if r varies in the range from

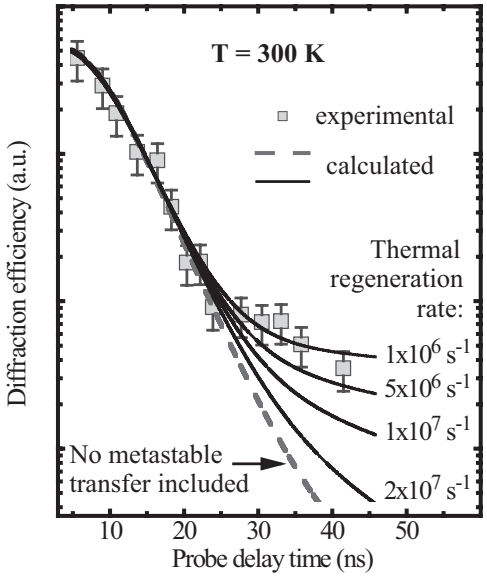

Fig. 8. Kinetics of the FWM signal in semiinsulating GaAs:EL2. Lines show the calculation results for different thermal regeneration rates

1×10^6 to $2 \times 10^6\,\mathrm{s^{-1}}$. Using Eq. (12), we evaluate the vibrational-attempt-frequency r_0 to range from 8×10^{11} to $1.6 \times 10^{12}\,\mathrm{s^{-1}}$ which is in good agreement with the results obtained by photocurrent recovery measurements at $T < 140$ K [35, 36]. Thus, our result strongly implies that the EL2 recovery time $1/r$ increases exponentially with temperature up to 300 K.

3.3. Determination of Dominant Photocarriers in CdTe Crystals by DFWM

Codoping of CdTe:V or $Cd_xZn_{1-x}Te$:V crystals by shallow impurities modifies charge states of the deep vanadium trap, and consequently, alters carrier generation, transport, and recombination. We analyzed numerically excitation-dependent carrier generation and their transport, ranging from monopolar to bipolar one, role of light-induced space-charge field to carrier transport, and the subnanosecond dynamics of a free carrier optical nonlinearity at various grating periods Λ and/or excitation intensities [15, 16]. A novel technique to determine the type of dominant carriers photoexcited from deep traps in a photorefractive semiconductor was suggested [16]. The method is based on the analysis of excitation dependent grating diffusive decay time $\tau_D \sim \Lambda^2 D^{-1}$, or the effective diffusion coefficient D, when the intensity varies in the range below the bipolar

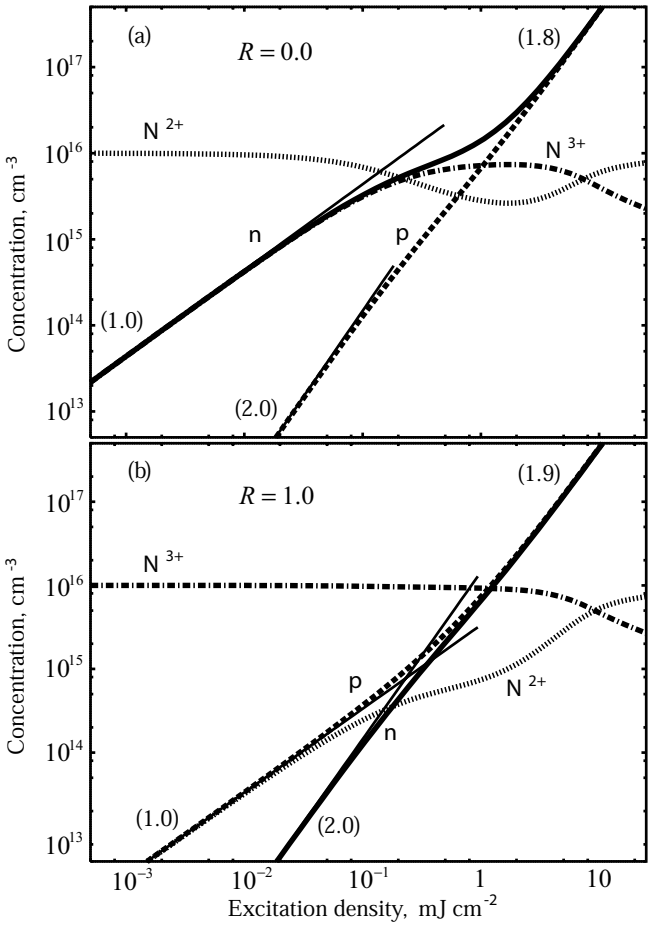

Fig. 9. Average density (zeroth Fourier components) of electrons n, holes p, neutral N^{2+}, and ionized N^{3+} traps as a function of excitation density calculated for two compensation ratios R of the deep trap. Numbers in brackets indicate the slope coefficients of the fits (thin solid lines) for the given dependences

carrier plasma limit. An increase (or decrease) of D with increasing excitation was a signature that electrons (or holes) are the major carriers photoexcited from deep traps.

Exposure characteristics are very informative if carrier generation, transport, or recombination have to be characterized [15, 31]. In particular, this is true for semiinsulating semiconductors when the charge state of a deep trap is significantly modified by optical excitation, but nonlinear excitation/recombination is still negligible. Several experimental regimes can be considered in time resolved measurements depending on the delay of a probe beam with respect to the exciting ones. For instance, the simultaneous excitation and probing is the most favorable regime to reveal carrier generation peculiarities. In contrast, when the probe delay exceeds a characteristic diffusion time of the carriers, the dependence on excitation density carries information on recombination processes. For our analysis, we have chosen an intermediate case, where both the carrier generation and transport determine the grating dynamics: the probe delay of $\Delta t = 180$ ps ensures that the carrier generation process by a 30 ps duration laser pulse is over and the nonequilibrium carrier transport dominates over recombination processes.

In Fig. 9, we compare the calculated dependences of deep impurity governed carrier generation vs. excitation energy for two different charge states of the vanadium impurity. These cases are labeled by different compensation ratios of a deep trap $R = N^{3+}/N_T$. Electron generation dominates in the case where a vanadium trap is totally neutral ($R = 0$) at excitations below 1 mJ cm^{-2}. In this case, hole generation requires the presence of the excited state N^{3+} which is created after the electron transition to the conduction band. Thus, the hole photoionization is intensity-dependent: $p \approx S_h N^{3+} \approx S_h S_e N^{2+} I^2$ and increases quadratically with excitation. Similarly, holes are major carriers in a crystal with $R = 1$, whereas electron photoionization exhibits a quadratic dependence of the exposure characteristic. On the other hand, a depletion of deep traps with excitation is evident and leads to the sublinear electron generation rate: the lower the compensation ratio, the more pronounced is the saturation of the electron generation rate. At excitations above 1 mJ cm^{-2}, the fluence becomes high enough for two-step transitions via the impurity level. The latter process eventually creates the equal densities of photoexcited electrons and holes and masks the initial different charge state of the impurity.

In spite of the fact that the deep-trap governed carrier generation extends from the monopolar case to bipolar one, the transport cannot be simply described by a gradual transfer from the monopolar to bipolar case. In order to reveal carrier transport related peculiarities, we have performed a hypothetical calculation with recombination processes excluded. The results of numerical analysis show (Fig. 10) that the electron grating, the one which is typically dominant in the free carrier optical nonlinearity, decays with monopolar diffusion time $\tau_{e,h} = \Lambda^2/4\pi^2 D_{e,h}$ at lowest excitations until the SC field builds up. Carrier drift in the field opposes the major carrier grating diffusive decay, therefore the τ_e value increases by few orders of magnitude with excitation. At excitations above 1 mJ cm^{-2}, which corresponds to nearly bipolar carrier generation, the grating decay time approaches the

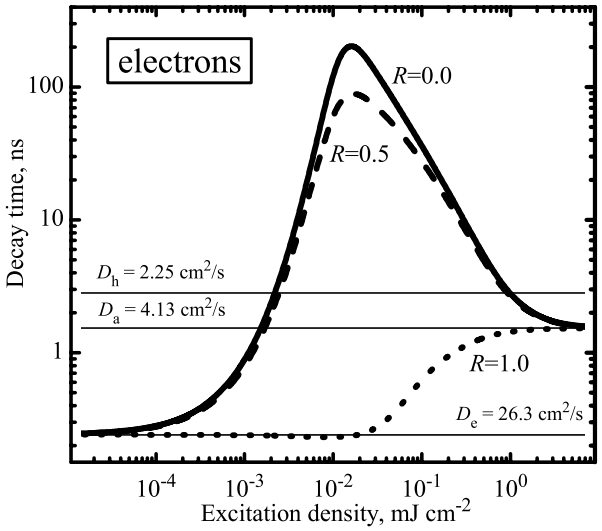

Fig. 10. Calculated decay times of the first Fourier component for electrons are shown for three compensation ratios R of a deep trap. Thin horizontal lines mark the bipolar and monopolar decay times with corresponding diffusion coefficients calculated for a 5 μm grating

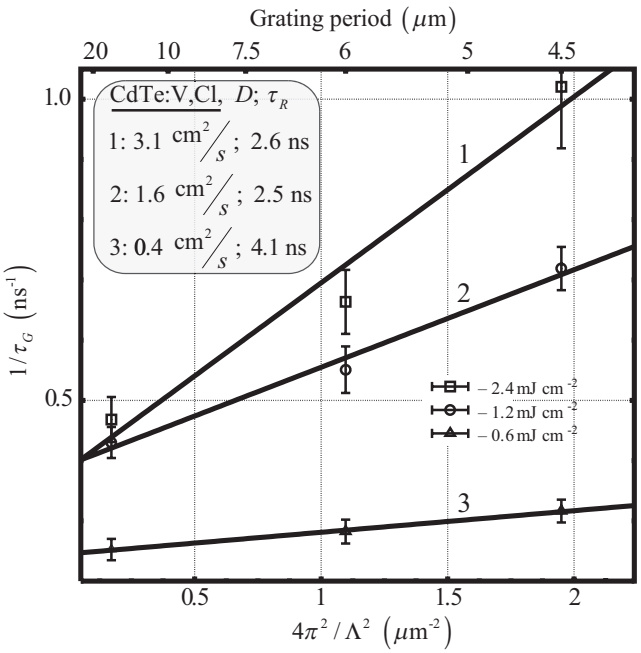

Fig. 11. Angular dependences of instantaneous grating decay time τ_G measured at 120 ps delay time at three excitation levels in Cl codoped CdTe:V crystal

bipolar diffusion time $\tau_{Da} = \tau_{De}\,\mu_e/\mu_a = \tau_{De}/[2(1+\mu_e/\mu_h)]$. To reach the latter case, the impurity-related SC field must be screened by the increasing carrier density.

We have calculated the angular dependences for a range of excitation intensities corresponding to a case which may be realized experimentally, i.e. in the vicinity of bipolar carrier generation and below it. The calculated slopes of dependences vary with excitation, which indicates different values of the effective diffusion coefficient D. At high excitations, the effective value of D was very close to a value of the bipolar carrier diffusion coefficient $D_a = 4.1\,\mathrm{cm^2\ s^{-1}}$ for all compensation ratios. However, for CdTe crystals with $R = 0$ and $R = 0.5$, the D value increased with excitation, whereas the D value decreased with excitation for the crystal with $R = 1$. This peculiarity — a decrease or increase of the effective D value with respect to the bipolar one with tuning the excitation intensity below the bipolar carrier generation level — was used to distinguish the type of nonequilibrium carriers in a photorefractive crystal.

This idea was verified experimentally by carrying out time-resolved four-wave mixing experiments in differently codoped CdTe:V and CdZnTe:V,As,Cl crystals [16]. Two sets of differently doped CdTe:V and $Cd_xZn_{1-x}Te$ samples were measured. The determined dominant type of photocarriers in photoexcited CdTe:V crystals correlated well with the carrier transport in CdTe:V samples with known density of neutral $[V^{2+}]$ and ionized $[V^{3+}]$ states. The type of photocarriers in $Cd_xZn_{1-x}Te$:V,Cl,As crystals was found from the dependence of the effective diffusion coefficient vs. excitation and correlated with the density of shallow donors and acceptors, determined by SIMS. As an example, in Fig. 11, we present the angular characteristics measured in CdTe:V,Cl sample. The plot of the angular dependence of the inverse grating decay time provided the diffusion coefficient value $D = 3.1\,\mathrm{cm^2\,s^{-1}}$ at the highest excitation, which corresponds to free carrier density of about $5 \times 10^{17}\,\mathrm{cm^{-3}}$. However, much smaller D values have been determined at lower excitations. The observed tendency to an increase in D with excitation clearly indicated that electrons are dominant photocarriers in CdTe:V,Cl sample, as is expected for a case of the totally filled $[V^{2+}]$ state.

Analogous measurements of CdTe:V,As crystal at the same excitation levels provided diffusion coefficients in the range of 8–12 $\mathrm{cm^2\ s^{-1}}$. The determined D values being much higher than the bipolar ones indicated that the SC field does not affect electron transport, as the field originates between holes and recharged deep traps.

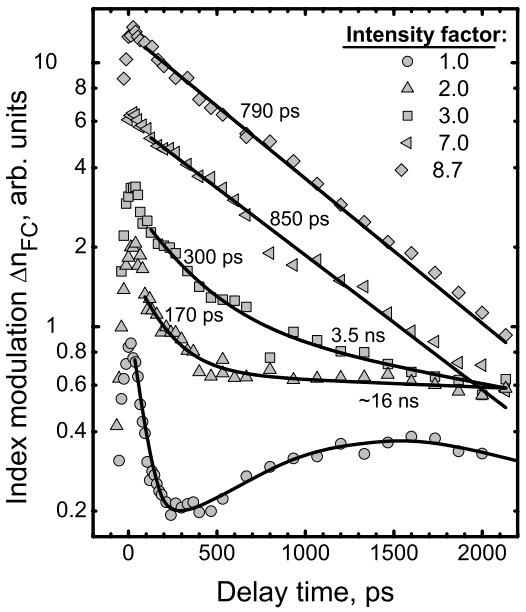

Fig. 12. Kinetics of light–induced refractive index modulation by free carriers is shown for different excitation levels. Intensity factor of 1 corresponds to 0.25 mJ/cm^2

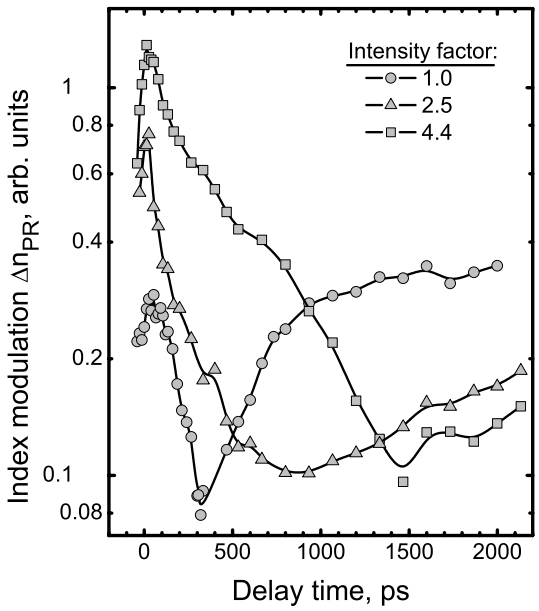

Fig. 13. Kinetics of light–induced refractive index modulation by SC field is shown for different excitation levels. Intensity factor of 1 corresponds to 0.4 mJ/cm^2.

Therefore, electrons are minority carriers, generated by two-step transitions. This leads to the conclusion that the hole generation should dominate at low excitations in an As-codoped crystal.

3.4. Sub-nanosecond Transients in SC Field Dynamics of CdTe:Ge Crystals

Application of a time-resolved picosecond photodiffractive technique for the investigation of the nonequilibrium carrier and space-charge field dynamics allowed us to observe some novel features in carrier generation and recombination processes, not typical of vanadium-doped CdTe crystals [15]. Namely, a fast capture of electrons in CdTe:V as well as the enhanced electron generation rate in Cl-codoped CdTe:V indicated the presence of other defects and complexes, in addition to the deep vanadium impurity.

We have extended the application of time-resolved photodiffractive techniques for the studies of Ge-doped CdTe crystals [38]. The samples were grown by the Bridgman technique, and had the dark resistivity of 10^8 — 10^9 Ωcm. We used a picosecond YAG laser, operating at 1.06 μm wavelength, to record and probe transient gratings. Free carrier and photorefractive gratings with spacing of 4.9 μm and the grating vector oriented along [110] axis of the photorefractive-cut crystal have been recorded. The contribution to diffraction by these two coexisting gratings was separated by using the anisotropy effect of diffraction on PR gratings [17,18,39]. The decays of FC and PR gratings were measured at different excitation energies in the range 0.3 to 3 mJ/cm^2.

A very peculiar FC and SC field sub-nanosecond dynamics, strongly dependent on excitation energy, has been observed. At excitations as low as 0.25 mJ/cm^2, the free carrier grating decays very fast, exhibits a dip at $\approx$ 500 ps, and then partially recovers with time (Fig. 12). With increasing excitation, the fast transient becomes slower, the dip disappears, and the grating decay is eventually described by a single exponential with a time constant of about 800 ps. Decay of the photorefractive grating is also composed of two parts (Fig. 13): at low excitations, it exhibits a similar dip and recovers slowly to the initial strength. At the highest excitations, it becomes more monotonous and is described by a time constant of 870 ps.

We attribute the dip in the FC dynamics to the contribution of a deep trap with high electron capture cross-section, the recombination activity of which saturates with excitation. The presence of centers for fast electron capture in CdTe:Ge, as "electron killers"

was reported in [40], and this effect may be governed by a number of complex defects, including Ge^+ state. A clear signature of electron capture is a very fast initial decay component which gradually disappears at higher intensities. Saturation of these fast "X" traps allows us to estimate their density, assuming that the photogenerated electron concentration becomes high enough to saturate this channel. From the diffraction efficiency of FC grating, we estimate an "X" trap density of about $(1 \div 3) \times 10^{15}\,\mathrm{cm}^{-3}$ [38].

In order to simulate the dynamics of these transients, we have performed numerical calculations by solving a system of charge balance equations using the two-deep trap model [41] with the system of balance equations modified by taking into account the spectroscopic studies of deep Ge centers by different techniques [40,42, 43]. The calculations confirmed the main tendencies in the vicinity of dips: for the FC nonlinearity, the slowly increasing Δn_{FC} value after the dip and, for the PR nonlinearity, a shift of the dip position to later times with excitation. The latter effect was shown to be due to increasing electron and hole density, which leads to the competition of the SC field in deep traps with the Dember field [38].

3.5. Nonequilibrium Carrier Dynamics in ZnTe

Recently, large (up to 3-inch in diameter) ZnTe single crystals of a high structural quality which were grown by the vertical gradient freezing (VGF) method became available [44]. These crystals can be easily p-type doped by phosphorus to achieve net hole concentrations in the 10^{17}—$10^{18}\,\mathrm{cm}^{-3}$ range. The possibility of realizing a vertical p-i-n diode by using these highly conductive p-type ZnTe substrates brings a distinct fabrication advantage over conventional III—V based devices on highly insulating sapphire, the latter requiring complex design and processing steps to provide the lateral electrical contacting of the device.

FWM measurements were performed at room temperature on VGF-grown ZnTe:P and undoped wafers (the latter with resistivity of $1 \cdot 10^3\,\Omega$cm). Phosphorus concentration in the ZnTe:P wafers ranged between 7×10^{17} and $1.5 \cdot 10^{18}\,\mathrm{cm}^{-3}$. The nonequilibrium carrier gratings were formed in the samples by two interfering 25 ps pulses, produced by an optical parametric oscillator at 500 nm or 566 nm wavelength, i.e., exciting the ZnTe crystals above or below the bandgap. The grating decay was monitored by a third (probe) pulse at 1064 nm wavelength, which was delayed up to 1 ns with respect to the recording (pump) beams.

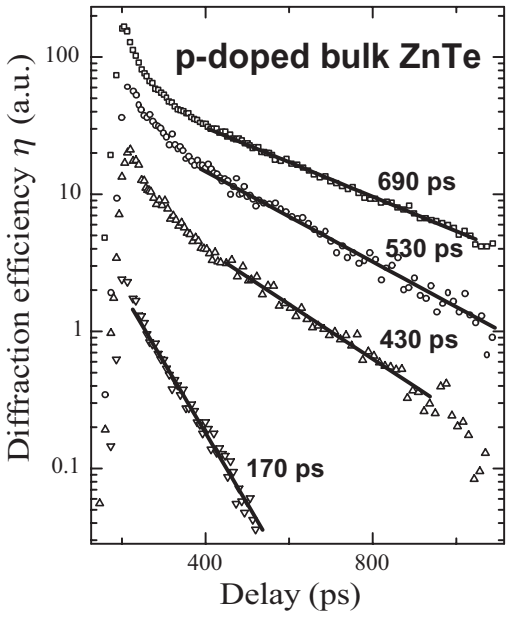

Fig. 14. Free carrier grating kinetics in p-doped ZnTe is shown at four excitation levels: 0.12, 0.24, 0.53 and 1 mJ/cm^2. The grating period is $\Lambda = 11\,\mu$m. Numbers in the plot show the grating decay times obtained from the exponential fits of the data from characteristic time intervals

In Fig. 14, we show the grating decay kinetics measured at the "surface" in p-doped ZnTe at different excitation levels. At lowest excitation intensity, the grating decays exponentially with $\tau_G = 170$ ps decay time, but, for higher excitations, the decay becomes slower (τ_G increases up to 690 ps at 1 mJ/cm^2). Such a carrier relaxation behaviour can be ascribed to the electrical activity of some type of defects in the crystal. These defects act as carrier trapping centers [15] which are nearly saturated at 1 mJ/cm^2 excitation intensity. Compensation of native defects could be also indirectly related to this finding through the proposed formation of a deep center by excess phosphorus in VGF-grown ZnTe:P [45].

Though analogous measurements in undoped ZnTe wafer have also shown the tendency for τ_G to increase with excitation from 120 to 160 ps, the range of τ_G variation is much smaller than that for ZnTe:P. Moreover, the grating decay kinetics was single-exponential for all excitations. These observations lead to the conclusion that the defect concentration in the p-doped wafer is lower than that in the undoped one, as

the trapping centers cannot be saturated in the latter case by a pump beam intensity around 1 mJ/cm^2.

We also measured the grating kinetics in the volume of the ZnTe:P wafer, using excitation at 566 nm, thus creating nonequilibrium carriers with densities in the range of 10^{16} cm^{-3}. At all excitation intensities, the grating decay was exponential with τ_G in the 600–700 ps interval. Thus, contrary to the "surface" grating case, we have not observed any fast carrier trapping. Under the latter conditions, with a considerably smaller concentration of free carriers (with respect to the surface excitation), the grating decay should exhibit a fast carrier trapping if a high density of homogeneously distributed defects was present in the crystal. Instead, the different grating decays observed within a few micron depth from the surface and in the volume of the ZnTe:P wafer can be explained assuming that the defect density is higher in the near-surface region of the wafer, while the rest of the crystal remains almost free of these defects, giving rise to relatively longer decays.

4. Four-wave Mixing in Heterostructures

In the present part, we review most recent results to indicate FWM applications for the investigation of layered structures. The range of materials studied extends from epitaxial layers in hetero- or homostructures to multilayered quantum confined structures, and the optical nonlinearities explore mechanisms of excitonic absorption, free carrier nonlinearity, or the quadratic electrooptic effect in an external dc-field [46]. As in the previous part, we consider mainly the case of nonresonant interaction and its potential applications for materials research. The early studies using non-degenerate FWM allowed the investigation of the carrier dynamics in the surface region of a semiconductor and the determination of the surface recombination velocity. For this case, the grating was recorded by picosecond laser pulses at a wavelength above the bandgap, and probed at a wavelength, to which the crystal was transparent. This allowed one to monitor the total density of carriers and reveal the contribution of surface recombination to the carrier dynamics within the first 100–200 ps, until they were localized near the surface. This approach was used to determine S values in bulk GaAs and InP [19] and monitor the surface quality after different etching, polishing, and doping procedures [47]. This configuration was applied later for studies of MOCVD-grown epitaxial $\sim$ 1 μm thick CdTe layers in the structure CdTe/ZnTe/GaAs and determine carrier parameters [48]. In addition to S, the values of carrier diffusion coefficient D and carrier lifetime within the CdTe layer were determined. The value of D was found few times higher than the expected bipolar one, and was attributed to monopolar carrier diffusion after the fast trapping of photoexcited electrons. A role of the ZnTe buffer layer was also studied by direct measurements of the carrier dynamics in it [49]. It is worth to note that the fast growth of 15–30 μm thick CdTe layers by the HVPE-method resulted in strained layers with a high density of dislocations and subsequent 300 ps carrier lifetimes. Indeed, the bimolecular carrier recombination at dislocations was observed in the exposure characteristics of diffraction, which indicated the sublinear carrier density dependence on excitation ($N \propto I^{1/2}$) [49]. Recently, this technique was used to study nitride semiconductor layers, as epitaxial GaN/sapphire, GaN/AlN/SiC, as well as LED structures of InGaN/GaN/sapphire. The determined value of D varied from 0.16 [50] to 1.7–2 cm^2/s [51] in accordance with the density of dislocations. Indeed, the recent studies of MOCVD-grown thick GaN layers with ultralow dislocation density resulted in a D value above 2 cm^2/s. The defect-related transport features were confirmed by measurements of carrier lifetime, which increased from 50–100 ps to few nanoseconds in 5–10 μm thick GaN epilayers. In case of InGaN/GaN layers, the buffer GaN layer (with larger bandgap than that of InGaN) confined photoexcited carriers in the front layer and thus allowed the studies of carrier transport and recombination features in a 50-nm thick InGaN layer [52]. The FWM configurations with counterpropagating pump-beams have been explored to study the perpendicular carrier transport in a MQWS [53]. In addition, polarization gratings recorded by perpendiculary-polarized beams, have been used to create spin-gratings and monitor the electron transport [12]. The potential applications of these novel modulation mechanisms and geometries for the metrology of semiconductor nanostructures are under investigation [54].

5. Holo-devices for Nondestructive Control of Semiconductors

Studies of photoelectrical properties and optical nonlinearities at Vilnius University resulted in the development of the free carrier transient grating technique and its applications for the nondestructive studies of technologically important materials. We foresee useful applications of the time-resolved FWM

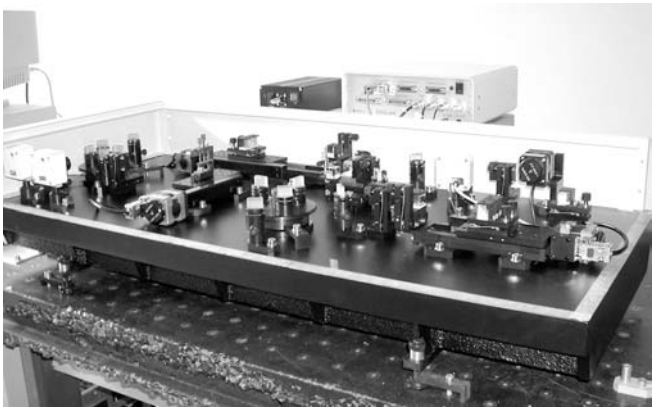

Fig. 15. A pilot device HOLO–1 (Ekspla Co.) for nondestructive control of bulk crystals, based on DFWM at 1.06 μm

technique for the control of wide bang gap materials, both bulk wafers and heterostructures. Recently, we implemented the picosecond FWM technique into devices and assembled (jointly with Ekspla Co, www.ekspla.com) two types of HOLO-devices, which can be attached to a pulsed laser source. Novel devices (Fig. 15) are able to control photoelectrical properties of bulk materials or heterostructures, using one or two fixed wavelengths and the advanced data acquisition system. The feasibility of the picosecond FWM technique on free carrier gratings has been demonstrated in numerous experiments. These studies allowed the implementation of the FWM technique and algorithms for parameter determination into novel customized HOLO-1 and HOLO-2 devices (Ekspla Co.) for the contactless control of technology-related photoelectric responses as well as for the metrology of nonequilibrium carrier parameters in bulk crystals and layered structures.

The research was sponsored by NATO's Scientific Affairs Division in the framework of the Science for Peace Programme (Project SfP-974476), European Commission (Contract No. G5MA-CT-2002-04047), and Lithuanian State Science and Studies Foundation. The authors would like to thank co-workers Dr. V. Gudelis, V. Mizeikis, R. Aleksiejunas, and T. Malinauskas for the contribution and acknowledge the cooperation links with research laboratories in France, Germany, Italy, Ukraine, Sweden, USA, Japan, and others which provided modern semiconductor materials.

1. *Shah J.* Ultrafast Spectroscopy of Semiconductors and Semiconductor Nanostructures. — Berlin: Springer, 1999.
2. *Chantre A., Vincent G., Bois D.*// Phys. Rev. B. — 1981. — **23**. — P. 5335.
3. *Martin G.M.*// Appl. Phys. Lett. — 1981. — **39**. — P. 747.
4. *Dabrowski J., Scheffler M.*// Phys. Rev. B. — 1989. — **40**. — P. 10391.
5. *Jain R. K., Klein M. B.*// Optical Phase Conjugation/Ed. by R.A. Fischer. — New York: Acad. Press, 1983. — P. 307—415.
6. *Eichler H. J., Günter P., Pohl D.W.* Laser-induced Dynamic Gratings. — Berlin: Springer, 1986.
7. *Special* Issue on Dynamic Gratings and Four-wave Mixing. IEEE J. Quant. Electron., 1986, **QE-22**.
8. *Ryskin A. I., Shcheulin A. S., Miloglyadov E. V.*// J. Appl. Phys. — 1998. — **83**. — P. 2215.
9. *Nolte D. D.*// Ibid. — 1996. — **79**. — P. 7514.
10. *Delaye P., Sugg B.*// Phys. Rev. B. — 1994. — **50**. — P. 16973.
11. *Kirkpatrick C. G., Chen R. T., Holmes D. E. et al.*// Semiconductors and Semimetals/ Ed. by R.K. Willardson, A.C. Beer. — New York: Acad. Press, 1984. — P. 159—231.
12. *Miller A.*//Nonlinear Optics in Semiconductors II/Ed. by E. Garmire, A. Kost. — San Diego: Acad. Press, 1999. — P. 287—312.
13. *Millerd J. E., Ziari M., Partovi A.*// Nonlinear Optics in Semiconductors I/Ed. by E. Garmire, A. Kost. — San Diego: Acad. Press, 1999. — P. 319—401.
14. *Smirl A. L., Valley G. C., Bohnert K. M. et al.*// IEEE J. Quant. Electron. — 1988. — **24**. — P. 289.
15. *Jarasiunas K., Bastiene L., Launay J. C. et al.*// Semicond. Sci. Technol. — 1999. — **14**. — P. 48.
16. *Sudzius M., Aleksiejunas R., Jarasiunas K. et al.*// Ibid. — 2003. — **18**. — P. 367.
17. *Schroeder W. A., Stark T. S., Boggess T. F. et al.*// Opt. Lett. — 1991. — **16**. — P. 799.
18. *Fabre J. C., Brotons E., Halter P. U. et al.*// Intern. J. Optoelectron. — 1989. — **4**. — P. 459.
19. *Hoffman C. A., Jarašiūnas K., Gerritsen H. J. et al.*// Appl. Phys. Lett. — 1978. — **33**. — P. 536.
20. *Manasreh M. O., Fischer D. W., Mitchel W. C.*// Phys. status solidi (b). — 1989. — **154**. — P. 11.
21. *Baraff G. A., Schluter M. A.*// Phys. Rev. B. — 1992. — **45**. — P. 8300.
22. *Vaitkus J., Gaubas E., Jarašiūnas K.*// Semicond. Sci. Technol. — 1992. — **7**. — P. A131.
23. *Jarašiūnas K., Vaitkus J., Bastienė L. et al.*// Proc. European Gallium Arsenide and Related III—V Compounds Applications Symposium, 1994. — P. 127–130.
24. *Juodkazis S., Vanagas E., Netikšis V. et al.*// Mater. Sci. Eng. B. — 1994. — **28**. — P. 448.
25. *Jarašiūnas K., Vaitkus J., Gaubas E. et al.*// Optical Diagnostics of Materials and Devices for Opto-, Micro-, and Quantum Electronics/ Ed. by S.V. Svechnikov, M.Y. Valakh. — (Proc. SPIE. — Vol. 2648. — 1995. — P. 538—544.)
26. *Sūdžius M., Gudelis V., Aleksiejūnas R. et al.*// Selected Papers on Optics and Photonics: Optical Diagnostics of Materials and Devices for Opto-, Micro-, and Quantum Electronics/Ed. by S.V. Svechnikov, M.Y. Valakh. — (Proc. SPIE. — Vol. 5024. — 2003. — P. 145—156.)

27. *Jarasiunas K., Lovergine N.*// Mater. Sci. Eng. B. — 2002. — **91**. — P. 100.

28. *Mizeikis V., Jarasiunas K., Gudelis V. et al.*// Mater. Sci. Forum. — 1999. — **279-2**. — P. 115.

29. *Nolte D. D., Olson D. H., Glass A. M.*// Phys. Rev. B. — 1989. — **40**. — P. 10650.

30. *Khromov A. L., Petrov M. P.*// Opt. Communs. — 1992. — **88**. — P. 315.

31. *Sūdžius M., Bastys A., Jarašiūnas K.*//Ibid. — 1999. — **170**. — P. 149.

32. *Jarašiūnas K., Vaitkus J., Delaye P. et al.*// Opt. Lett. — 1994. — **19**. — P. 1946.

33. *Fischer D. W.*// Appl. Phys. Lett. — 1987. — **50**. — P. 1751.

34. *Vincent G., Bois D., Chantre A.*// J. Appl. Phys. — 1982. — **53**. — P. 3643.

35. *Mitonneau A., Mircea A.*// Solid State Communs. — 1979. — **30**. — P. 157.

36. *Kristensen I. K., Møller S.*// Ibid. — 1996. — **99**. — P. 751.

37. *Aleksiejunas R., Sudzius M., Jarasiunas K.*// Opt. Communs. — 2001. — **198**. — P. 115.

38. *Jarašiūnas K., Sūdžius M., Aleksiejūnas R. et al.*// Trends in Optics and Photonics Series. — 2001. — **62**. — P. 246.

39. *Jarašiūnas K., Delaye P., Roosen G.*// Phys. status solidi (b). — 1993. — **175**. — P. 445.

40. *Sharager C., Siffert P., Hoschl P. et al.*// Phys. status solidi (a). — 1981. — **66**. — P. 87.

41. *Delaye P., de Montmorillon L. A., Biaggio I. et al.*// Opt. Communs. — 1997. — **134**. — P. 580.

42. *Briat B., Ramaz F., Farid B. et al.*// J. Cryst. Growth. — 1999. — **197**. — P. 724.

43. *Shcherbin K., Shumeljuk A., Odoulov S. et al.*// Optical Diagnostics of Materials and Devices for Opto-, Micro-, and Quantum Electronics/ Ed. by S.V. Svechnikov, M.Y. Valakh. — (Proc. SPIE. — Vol. 2795. — 1996. — P. 236.)

44. Sato K., Hanafusa M., Noda A. et al.// J. Cryst. Growth. — 2000. — **214**. — P. 1080.

45. *Asahi T., Arakawa A., Sato K.*// Ibid. — 2001. — **229**. — P. 74.

46. *Nolte D. D.*// J. Appl. Phys. — 1999. — **85**. — P. 6259.

47. *Hoffman C. A., Gerritsen H. J., Nurmikko A. V.*// Ibid. — 1980. —**51**. — P. 1603.

48. *Mizeikis V., Jarasiunas K., Lovergine N. et al.*// J. Cryst. Growth. — 2000. — **214**. — P. 234.

49. *Jarasiunas K., Gaubas E., Aleksiejunas R. et al.*// Phys. status solidi (a). — 2003. — **195**. — P. 238.

50. *Haag H., Honerlage B., Briot O. et al.*//Phys. Rev. B. — 1999. — **60**. — P. 11624.

51. *Aleksiejunas R., Sudzius M., Malinauskas T. et al.*// Appl. Phys. Lett. — 2003. — **83**. — P. 1157.

52. *Aleksiejūnas R., Sūdžius M., Gudelis V. et al.*// Phys. status solidi (c). — 2003 (DOI 10.1002/pssc.200303261).

53. *Norwood D. P., Smirl A. L., Swoboda H. E.*// J. Appl. Phys. — 1995. — **77**. — P. 1113.

54. *Jarasiunas K., Gudelis V., Aleksiejunas R. et al.*//Appl. Phys. Lett. — 2004. — **84**. — P. 1043.

ОПТИЧНІ НЕЛІНІЙНОСТІ ОБ'ЄМНИХ НАПІВПРОВІДНИКІВ, ЗУМОВЛЕНІ ГУСТИНОЮ ТА ТРАНСПОРТНИМИ ВЛАСТИВОСТЯМИ НОСІЇВ ЗАРЯДУ

М. Судзіус, К. Ярашюнас

Р е з ю м е

Описано розвиток методики чотирихвильової взаємодії на вільних носіях та фоторефрактивних перехідних гратках в об'ємних напівпровідникових матеріалах. Експериментальні дослідження поряд з числовим моделюванням дозволили продемонструвати застосовність методик нано- та пікосекундних динамічних граток для контролю якості напівпровідникових підкладок, для дослідження фотоподавлення EL2-дефектів в GaAs при кімнатній температурі, а також для виявлення умов, в яких зворотний зв'язок поля просторового заряду ефективно впливає на перенос заряду в кристалах GaAs, CdTe та ZnTe, легованих різними домішками.